

Dual Network Architecture for Few-view CT – Trained on ImageNet Data and Transferred for Medical Imaging

Huidong Xie, Hongming Shan, Wenxiang Cong, Xiaohua Zhang, Shaohua Liu, Ruola Ning,
Ge Wang

ABSTRACT

X-ray computed tomography (CT) reconstructs cross-sectional images from projection data. However, ionizing X-ray radiation associated with CT scanning might induce cancer and genetic damage and raises public concerns. Therefore, the reduction of radiation dose has attracted major attention. Few-view CT image reconstruction is an important topic to reduce the radiation dose. Recently, data-driven algorithms have shown great potential to solve the few-view CT problem. In this paper, we develop a dual network architecture (DNA) for reconstructing images directly from sinograms. In the proposed DNA method, a point-wise fully-connected layer learns the backprojection process requesting significantly less memory than the prior art and with $O(C \times N \times N_c)$ parameters where N and N_c denote the dimension of reconstructed images and number of projections respectively. C is an adjustable parameter that can be set as low as 1. Our experimental results demonstrate that DNA produces a competitive performance over the other state-of-the-art methods. Interestingly, natural images can be used to pre-train DNA to avoid overfitting when the amount of real patient images is limited.

Keywords: Dual network architecture (DNA), generative adversarial network (GAN), few-view CT, sparse-view CT, machine learning, deep learning.

1. INTRODUCTION

Few-view CT is often mentioned in the context of tomographic image reconstruction. Because of the requirement imposed by the Nyquist sampling theorem, reconstructing high-quality CT images from under-sampled data was considered impossible. When sufficient projection data are acquired, analytical methods such as filtered back-projection (FBP) [1] are widely used for clinical CT image reconstruction. In few-view CT circumstance, severe streak artifacts are introduced in these analytically reconstructed images due to the incompleteness of projection data. In order to overcome this issue, various iterative techniques were proposed in the past decades, which can incorporate prior knowledge in the image reconstruction. Well-known methods include algebraic reconstruction technique (ART) [2], simultaneous algebraic reconstruction technique (SART) [3], expectation maximization (EM) [4], etc. Nevertheless, these iterative methods are time-consuming and still not able to produce satisfying results in many cases. Recently, the development of the graphics processing unit (GPU) technology and the availability of big data allow researchers to train deep neural networks in an acceptable amount of time. Therefore, deep learning has become a new frontier of CT reconstruction research [5][6][7].

In the literature, only a few deep learning methods were proposed for reconstructing images directly from raw data. Zhu et al. [8] use fully-connected layers to learn the mapping from raw k-space data to a corresponding reconstructed MRI image. There is no doubt that fully-connected layers can learn the mapping from the sinogram domain to the image domain. However, importing the whole sinograms into the network requires a significant amount of memory and poses a major challenge to train the network for a full-size CT image/volume on a single consumer-level GPU such as an NVIDIA Titan Xp. A recently proposed method, iCT-Net [9], reduces the computational complexity from $O(N^4)$ in [8] to $O(N^2 \times N_c)$, where N and N_c denote the size of a medical image and the number of projections respectively.

In this study, we propose a dual network architecture (DNA) for CT reconstruction, which reduces the required parameters from $O(N^2 \times N_c)$ of iCT-Net to $O(C \times N \times N_c)$, where C is an adjustable hyper-parameter much less than N , which can be even set as low as 1. Theoretically, the larger the C , the better the performance. The proposed network is trainable on one consumer-level GPU such as NVIDIA Titan Xp or NVIDIA 1080 Ti. The proposed DNA is inspired by the FBP formulation so as to learn a refined filtration backprojection process for reconstructing images directly from sinograms. For X-ray CT, every single point in the sinogram domain only relates to pixels/voxels on an X-ray path through a field of view. With this intuition, the reconstruction process of DNA is learned in a point-wise manner, which is the key ingredient of DNA to alleviate the memory burden. Also, the insufficient training dataset is another

major issue in deep imaging. Inspired by [8], we first pre-train the network using natural images from the ImageNet [10] and then fine-tune the model using real patient data. To our best knowledge, this is the first work using ImageNet images to pre-train a medical CT reconstruction network. In the next section, we present a detailed explanation of our proposed DNA network. In the third section, we describe the experimental design, training data and reconstruction results. Finally, in the last section we discuss relevant issues and conclude the paper.

2. METHODS

2.1 Generator networks

DNA consists of 2 generator networks, $G1$ and $G2$. The input to the $G1$ is a batch of few-view sinograms. According to the Fourier slice theorem, low-frequency information is sampled denser than high-frequency information. Therefore, if we perform backprojection directly, reconstructed images will become blurry. Ramp filter is usually used to filter projections to avoid this blurring effect. In DNA, the ramp filtration is performed on the sinogram in the Fourier domain through multiplication with the filter length twice the length of the sinogram (which can be shortened). Then, the filtered projections are fed into the first generator $G1$. $G1$ tries to learn a filtered backprojection algorithm and output an intermediate image. Then, $G2$ further optimizes the output from $G1$, generating the final image.

$G1$ can be divided into three components: filtration, backprojection, and refinement. In the filtration part, 1-D convolutional layers are used to produce filtered data. Theoretically, the length of the filter is infinitely long for a continuous signal, but it is not practical in reality. Since the filtration is done through a multi-layer CNN, different layers can learn different parts of the filter. Therefore, the convolution window is empirically set as $\frac{1}{4}$ the length of the projection vector in order to reduce the computational burden. The idea of residual connections is used to reserve low-level information and prevent gradient from vanishing.

Next, the learned sinogram from the filtration part are backprojected by $G1$. The backprojection part of $G1$ is inspired by the following intuition: every point in the filtered projection vector only relates to pixel values on the x-ray path through the corresponding object image and any other data points in this vector contribute nothing to the pixels on this x-ray path. There is no doubt that a single fully-connected layer can be implemented to learn the mapping from the sinogram to the image space, but its memory requirement becomes an issue due to extremely large matrix multiplications in this layer. In order to reduce the memory burden, the reconstruction process is learned in a point-wise manner using a point-wise fully-connected layer. By doing so, DNA can truly learn the backprojection process. The input to the point-wise fully-connected layer is each single point in the filtered projection vector, and the number of neurons is the width of the corresponding image. After this point-wise fully-connected layer, rotation and summation operations are applied to simulate the analytical FBP method. Bilinear interpolation [11] is used for rotating images. Moreover, C is empirically set as 23, allowing the network to learn multiple mappings from the sinogram domain to the image space. The number of C can be understood as the number of branches. Note that different view-angle uses different parameters. Although the proposed filtration and backprojection parts all together learn a refined FBP method, streak artifacts cannot be eliminated perfectly. An image reconstructed by the backprojection part is fed into the last portion of $G1$ for refinement.

$G1$ is a typical U-net [12] with conveying paths and built with the ResNeXt structure. U-net was originally designed for biological images segmentations and has been utilized in various applications and achieved an outstanding performance. For example, [13][14][15] uses U-net with conveying paths for CT-image denoising, [16][17] for few-view CT problem and [18] for compressed sensing MRI, etc. U-net in these proposed methods contains 4 down-sampling and 4 up-sampling layers, each has a stride of 2 and is followed by a rectified linear unit (ReLU). A 3×3 kernel is used in both convolutional and transpose-convolutional layers. The number of kernels in each layer is 36. In order to maintain the tensor's size, zero-padding is used.

$G2$ uses the same structure as the refinement part. The input to $G2$ is a concatenation of FBP-result and output from $G1$. With the use of $G2$, the network becomes deep. As a result, the benefits of deep learning can be utilized in this direct mapping for CT image reconstruction.

2.2 Discriminator network

WGAN [19] architecture with a gradient penalty is used to train the proposed DNA. The discriminator network takes input from $G1$, $G2$, and the ground-truth dataset, trying to distinguish whether the input is real or fake. In DNA, the discriminator network has 6 convolutional layers with 64, 64, 128, 128, 256, 256 filters and followed by 2 fully-

connected layers with number of neurons 1,024 and 1 respectively. The leaky ReLU activation function is after each layer with a slope of 0.2 in the negative part. The convolutional kernel 3×3 and zero-padding are used for all the convolutional layers, with stride equals 1 for odd layers and 2 for even layers.

2.3 Objective functions

The objective function for optimizing the generators involves the mean square error (MSE) [20] [21], structural similarity (SSIM) [22][23] and adversarial loss [24][25]. MSE is a popular choice for denoising applications [26], which effectively suppresses the background noise [26] but could result in over-smoothed images [27]. Moreover, MSE is insensitive to image texture since it assumes background noise is white Gaussian noise and independent of local image features [22]. In order to compensate for the disadvantages of MSE and acquire visually better images, SSIM is introduced in the objective function. Furthermore, the adversarial loss aims to assist the generators to produce sharp images that are indistinguishable by the discriminator network. As mentioned early, solving the few-view CT problem is similar to solving a set of linear equations when the number of equations is not sufficient to perfectly resolve all the unknowns. The intuition of DNA is trying to estimate those unknown as close as possible by combining the information from the existing equations and the knowledge hidden in the big data. The recovered unknowns should satisfy the equations we have. Therefore, MSE between the original sinogram and the synthesized sinogram from a reconstructed image (either $G1$ or $G2$) is also included as part of the objective function.

3. EXPERIMENTS AND RESULTS

3.1 Experimental design

The dataset is the clinical patient dataset generated and authorized by Mayo Clinics for “*the 2016 NIH-AAPM-Mayo Clinic Low Dose CT Grand Challenge*”[28]. The dataset contains a total of 5,936 abdominal CT images selected by Mayo Clinic with 1 mm slice thickness. Pixel values of patient images were normalized between 0 and 1. In this dataset, 9 patients (5,410 images) are for training and validation while 1 patient (526 images) is for testing. As mentioned early, DNA was first pre-trained using natural images from IMAGENET. During the pre-training segment, a total of 120,000 images were randomly selected from IMAGENET, among which 114,000 images were used for training and the remaining 6,000 images were used for validation/testing. Pixel values of IMAGENET images were also normalized between 0 and 1. All the pixel values outside a prescribed circle were set to 0. All images were resized to 256×256 . The Radon transform was used to simulate few-view projection measurements. 39-view and 49-view sinograms were respectively synthesized from angles equally distributed over a full scan range.

A batch size of 10 was selected for training. All experiments were implemented in the TensorFlow framework [29] on an NVIDIA Titan Xp GPU. The Adam optimizer was used to optimize the parameters [30]. We compared DNA with 3 state-of-the-art deep learning methods, including LEARN [31], sinogram-synthesis U-net [17], and iCT-Net [9]. To our best knowledge, the network settings are the same as the default settings described in the original papers.

For the LEARN network, the number of iterations λ^t was set as 50, the number of filters for all three layers were set to 48, 48, and 1 respectively. The convolutional kernel was set as 5×5 . The initial input to the network was the FBP result. The same preprocessed Mayo dataset described above was used to train the LEARN network. Please note that the amount of data we used to train the LEARN network was much larger than that in the original LEARN paper.

For the sinogram-synthesis U-net, 720-view sinograms were simulated using the Radon transform. Then, the simulated sinograms were cropped into 50×50 patches with a stride 10 for training. The FBP method was applied to the sinograms for generating final images.

The training process of iCT-Net is divided into two stages. In the first stage, the first 9 layers were pre-trained with projection data. In the second stage, the pre-trained iCT-Net performed the end to end training using the patient data. In the original iCT-Net paper, iCT-Net used a total of 58 CT examinations acquired under the same condition for the stage 2 training. However, since we do not have their dataset, limited Mayo images might had caused overfitting in the stage 2 training when we made efforts to replicate their results. Therefore, for fair comparison, testing images were included in the training stages. Please note that iCT-Net was handled by 2 NVIDIA Titan Xp GPUs.

3.2 Visual and quantitative assessment

In order to visualize the performance of different methods, a few representative slices were selected from the testing dataset. Figure 5 shows results reconstructed using different methods from 49-view real patient sinograms. Table. 1 shows the number of parameters used for these methods.

Table 1. The number of parameters used in different methods.

	LEARN	Sino-syn U-net	iCT-Net	DNA (49-views)	DNA (39-view)
# of parameters	3,004,900	47,118,017	16,933,929	1,962,101	1,844,341

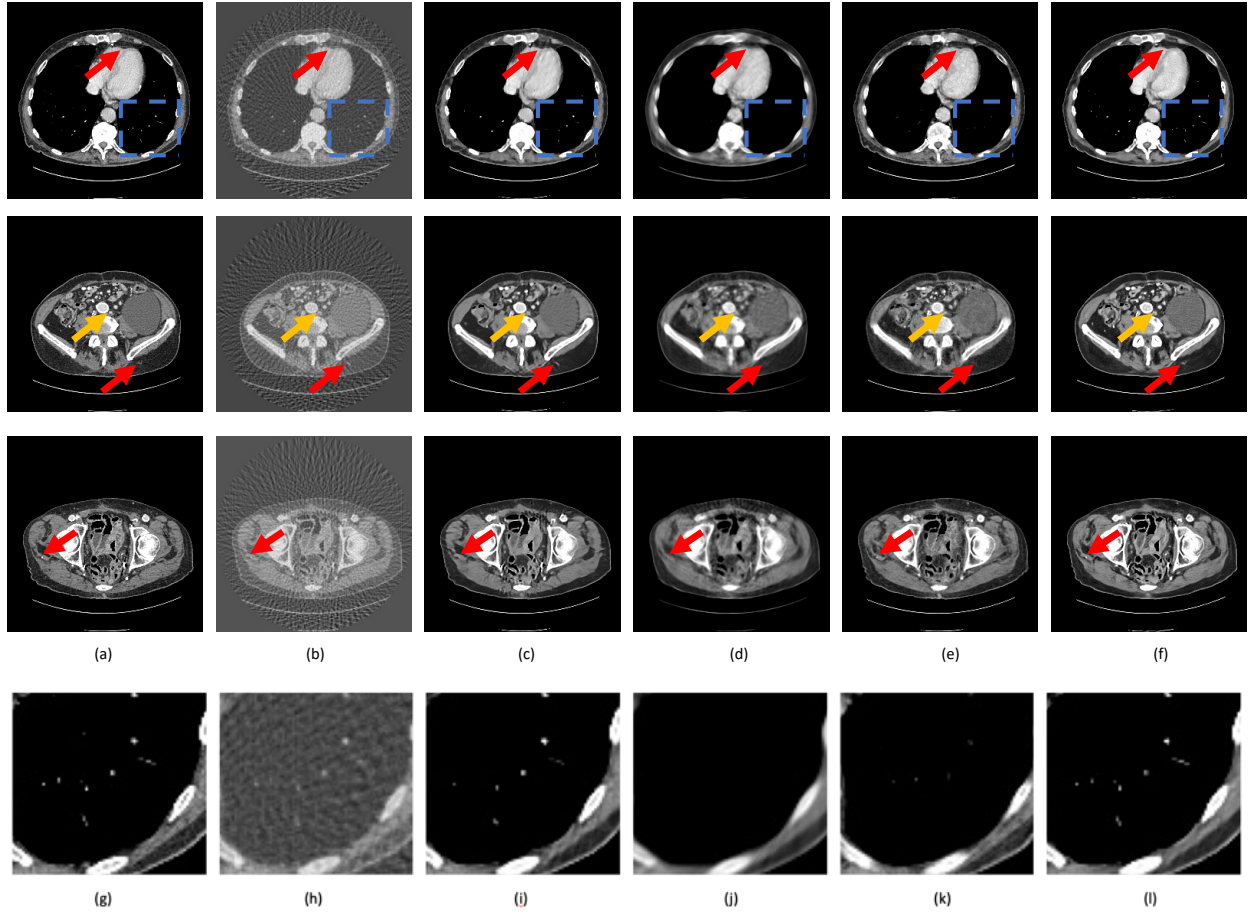


Figure. 1. Representative images reconstructed using different methods. The display window is $[-160, 240]$ HU for patient images. (a) The ground-truth, (b) FBP, (c) LEARN, (d) sinogram-synthesis U-net, (e) iCT-Net, (f) DNA. (g) – (l) The zoomed region of the first row marked by the blue boxes. More tiny details were recovered using our proposed method. The red arrows point to some small details better reconstructed by DNA.

For qualitative assessment, three metrics include PSNR, SSIM, and root-mean-square-error (RMSE). Table. 2 shows quantitative measurements for different methods, acquired by averaging the metrics over the testing dataset, for both 39-view and 49-view results.

Table 2. Quantitative measurements for different methods ($MEAN \pm STD$). For each metric, the best results are marked in red. We did not test the iCT-Net for the 39-view case. Measurements are acquired by averaging the values in the testing dataset.

	LEARN	Sino-syn U-net	iCT-Net	DNA
SSIM (49-views)	0.900 ± 0.026	0.814 ± 0.029	0.784 ± 0.020	0.913 ± 0.023
PSNR (49-views)	28.966 ± 1.262	24.858 ± 0.777	27.062 ± 0.904	29.174 ± 1.234
RMSE (49-views)	0.036 ± 0.006	0.057 ± 0.005	0.045 ± 0.005	0.035 ± 0.005
SSIM (39-views)	0.882 ± 0.029	0.781 ± 0.029		0.897 ± 0.026
PSNR (39-views)	27.994 ± 1.211	24.040 ± 0.753		28.294 ± 1.260
RMSE (39-views)	0.040 ± 0.006	0.063 ± 0.006		0.038 ± 0.006

3.3 Examination of intermediate results

In order to demonstrate the effectiveness of two generators in DNA, another $G2$ network was trained using solely the FBP results as the input. Figure. 8 shows typical results reconstructed from 49-view sinograms using various methods.

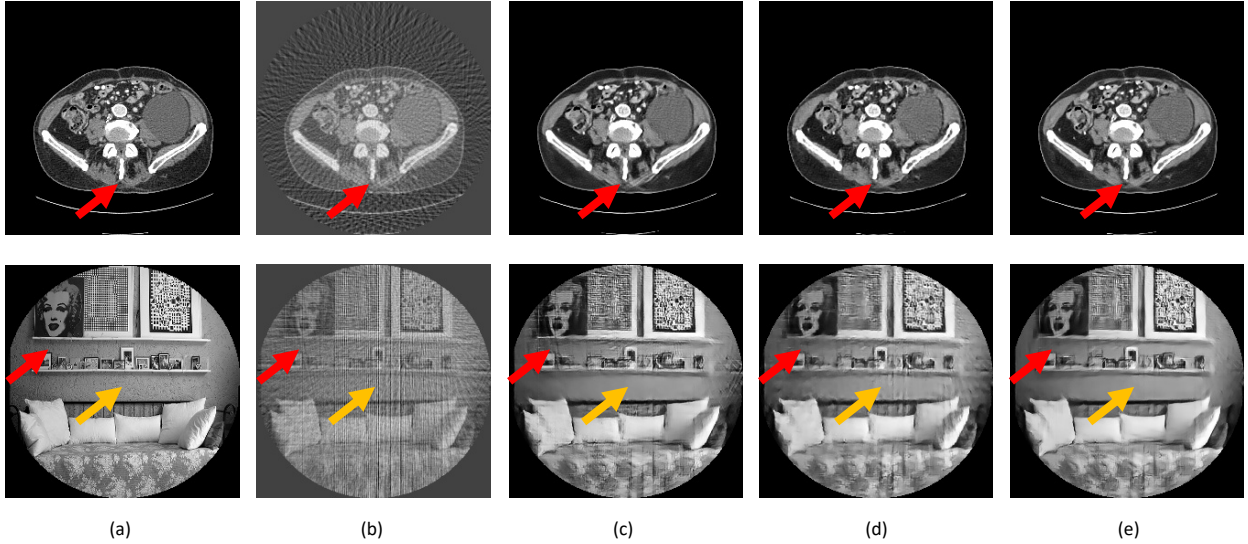


Figure. 2. Representative outputs using different methods. (a) The ground-truth, (b) FBP, (c) $G2$ trained using only FBP results as the input, (d) $G1$, and (e) DNA. The display window is $[-160, 240]$ HU for patient images.

As shown in the first row in Figure. 7, streak artifacts cannot be perfectly eliminated by $G2$ when the network is trained only using the FBP results. $G1$, on the other hand, eliminates these artifacts through learning from projection data (first row, red arrows). Moreover, as mentioned early, by the design $G1$ intends to assist $G2$ for producing better results. This effect can be observed in the second row of Figure 5. $G1$ removed artifacts that cannot be removed using $G2$ (second row, red arrow), but it introduces new artifacts (second row, orange arrow). The artifact was then removed by $G2$ that did not introduce artifacts that exist in images reconstructed by $G2$ without the assistance of $G1$. In summary, $G1$ helped remove artifacts that could not be removed by processing FBP results, even though it brought up new artifacts, the newly introduced artifacts can actually be removed by the second generator network. Put differently, the proposed method, DNA, combines the best of two worlds. Quantitative measurements on the outputs reconstructed by various components in DNA are listed in Table 4.

Table 3. Quantitative measurements for different components in DNA ($MEAN \pm STD$). The best results are marked in red. Measurements are acquired by averaging the values in the testing dataset.

	G1	G2 (trained using only FBP results)	DNA
SSIM (49-views)	0.899 ± 0.025	0.908 ± 0.023	0.913 ± 0.023
PSNR (49-views)	28.015 ± 1.111	28.789 ± 1.167	29.174 ± 1.234
RMSE (49-views)	0.040 ± 0.005	0.037 ± 0.005	0.035 ± 0.005

3.4 Generalizability analysis

In order to demonstrate that the proposed method truly learns the backprojection process and can be generalized to other datasets, DNA and LEARN (second best method) were tested directly on female breast CT datasets acquired on a breast CT scanner (Koning corporation). Totally, 4,968 CT images, scanned at 49 peak kilovoltage (kVp), were acquired from 12 patients. There is a total of 3 sets of images per patient, reconstructing from 300, 150, 100 projections respectively. Figure 8 shows representative images. Table 5 gives the corresponding quantitative measurements. Completely dark images in the dataset were excluded, resulting in a total of 4,635 CT images.

DNA demonstrates an outstanding performance in terms of generalizability, as shown in Figure 8. Specifically, images reconstructed using LEARN appear over-smoothed, losing some details. On the other hand, DNA not only reserves more details than LEARN but also suppresses streak artifacts effectively, relative to 150-view and 100-view results. Moreover, images reconstructed by DNA from 49-view sinograms are better than 100-view images in terms of both SSIM and RMSE.

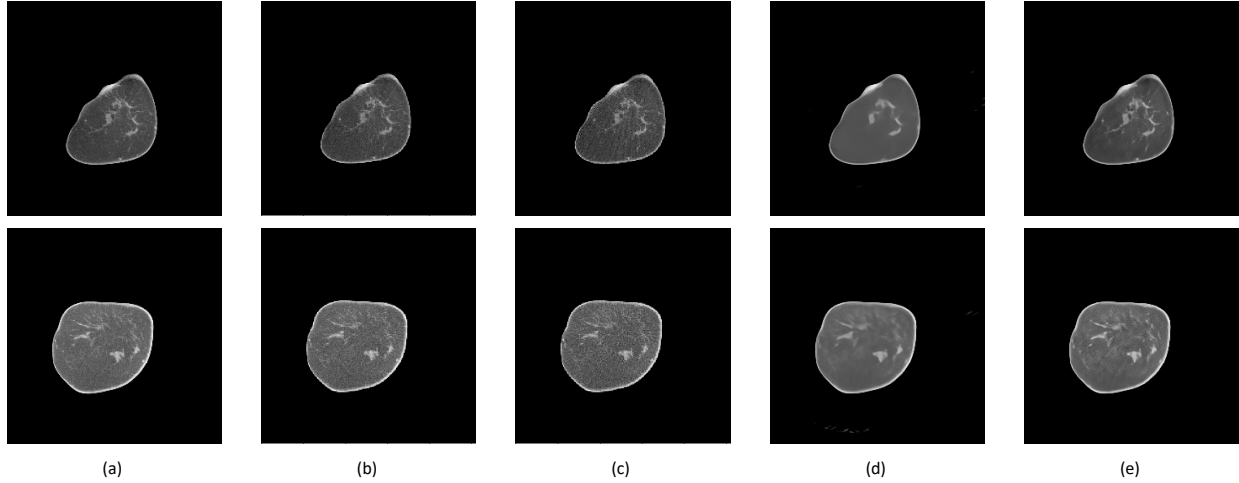


Figure 3. Representative outputs using different methods on Koning breast CT datasets. (a) Images reconstructed from 300-view, (b) 150-view, and (c) 100-view sinograms respectively; (d) LEARN and (e) DNA outputs respectively. The display window is $[-300, 300]$ HU.

Table 4. Quantitative measurements for Koning breast images reconstructed using different methods ($MEAN \pm STD$). Measurements were calculated with respect to 300-view results and acquired by averaging the values in the testing dataset. The best and second-best results are marked in red and blue respectively.

	150-view	100-view	LEARN	DNA (49-view)
SSIM	0.972 ± 0.038	0.953 ± 0.062	0.922 ± 0.076	0.957 ± 0.057
PSNR	42.455 ± 10.141	38.880 ± 10.022	34.588 ± 3.658	37.415 ± 4.259
RMSE	0.012 ± 0.010	0.018 ± 0.015	0.021 ± 0.011	0.015 ± 0.008

Also, we validated DNA and LEARN on the Massachusetts General Hospital (MGH) dataset [32]. MGH dataset contains 40 cadaver scans acquired with representative protocols. Each cadaver was scanned on a GE Discovery HD 750 scanner at 4 different dose levels. Only 40NI (Noise Index) images were used for testing. *NI* refers to the standard deviation of CT numbers within a region of interest in a water phantom of a specific size [33]. Typical images are shown in Figure. 9. The corresponding quantitative measurements are in Table 6.

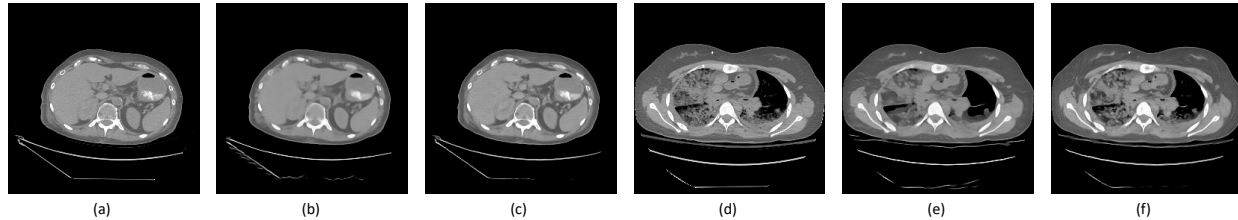


Figure. 4. Representative outputs using different methods for the MGH dataset from 49-view sinograms. (a) & (d) 40NI, (b) & (e) LEARN, (c) & (f) DNA. The display window is $[-300, 300]$ HU.

Table 5. Quantitative measurements for the MGH dataset reconstructed using different methods ($MEAN \pm STD$). Measurements were acquired by averaging the values in the testing dataset. The best results are marked in red.

	LEARN	DNA
SSIM (49-view)	0.849 ± 0.039	0.874 ± 0.039
PSNR (49-view)	26.193 ± 1.131	27.687 ± 1.566
RMSE (49-view)	0.049 ± 0.007	0.042 ± 0.008

4. CONCLUSION

Although the field of deep learning is still at its early stage, it has achieved remarkable results over the past several years. We envision that deep learning will play an important role in the field of tomographic imaging [34]. Along this direction, we have developed this novel DNA network for reconstructing CT images directly from sinograms. In this paper, the proposed method has only been tested for the few-view CT problem, we believe that it can be applied/adapted to solve various other CT problems, including image de-noising, limited-angle CT, and so on. This paper is not the first work for reconstructing images directly from raw data, but the previously proposed methods require a significantly greater amount of GPU memory for training. It is underlined that our proposed method solves the memory issue by learning the reconstruction process with the point-wise fully-connected layer and other proper network ingredients. For example, by dividing the point-wise fully-connected layer into multiple segments, the proposed DNA can be trained on a cheap GPU. Also, by passing only a single point into the fully-connected layer, the proposed method is able to truly learn the backprojection process. In our study, the DNA network demonstrates superior generalizability. In the future works, we will validate the proposed method on images up to dimensionality 512×512 or even 1024×1024 .

5. REFERENCES

- [1] G. Wang, Y. Ye, and H. Yu, "Approximate and exact cone-beam reconstruction with standard and non-standard spiral scanning," *Phys Med Biol*, vol. 52, no. 6, pp. R1-13, Mar. 2007.
- [2] R. Gordon, R. Bender, and G. T. Herman, "Algebraic reconstruction techniques (ART) for three-dimensional electron microscopy and x-ray photography," *Journal of theoretical biology*, vol. 29, no. 3, pp. 471-481, 1970.
- [3] A. Andersen, "Simultaneous Algebraic Reconstruction Technique (SART): A superior implementation of the ART algorithm," *Ultrasonic Imaging*, vol. 6, no. 1, pp. 81-94, Jan. 1984.
- [4] A. P. Dempster, N. M. Laird, and D. B. R. R. work(s), "Maximum Likelihood from Incomplete Data via the EM Algorithm," *Journal of the Royal Statistical Society. Series B (Methodological)*, vol. 39, no. 1, pp. 1-38, 1977.
- [5] G. Wang, "A Perspective on Deep Imaging," *IEEE Access*, vol. 4, pp. 8914-8924, 2016.
- [6] G. Wang, A. Butler, H. Yu, and M. Campbell, "Guest Editorial Special Issue on Spectral CT," *IEEE Transactions on Medical Imaging*, vol. 34, no. 3, pp. 693-696, Mar. 2015.

- [7] G. Wang, J. C. Ye, K. Mueller, and J. A. Fessler, "Image Reconstruction is a New Frontier of Machine Learning," *IEEE Trans Med Imaging*, vol. 37, no. 6, pp. 1289–1296, 2018.
- [8] B. Zhu, J. Z. Liu, S. F. Cauley, B. R. Rosen, and M. S. Rosen, "Image reconstruction by domain-transform manifold learning," *Nature*, vol. 555, no. 7697, pp. 487–492, Mar. 2018.
- [9] Y. Li, K. Li, C. Zhang, J. Montoya, and G. Chen, "Learning to Reconstruct Computed Tomography (CT) Images Directly from Sinogram Data under A Variety of Data Acquisition Conditions," *IEEE Transactions on Medical Imaging*, pp. 1–1, 2019.
- [10] "ImageNet." [Online]. Available: <http://image-net.org/index>. [Accessed: 19-Apr-2019].
- [11] K. T. Gribbon and D. G. Bailey, "A novel approach to real-time bilinear interpolation," in *Proceedings. DELTA 2004. Second IEEE International Workshop on Electronic Design, Test and Applications*, 2004, pp. 126–131.
- [12] O. Ronneberger, P. Fischer, and T. Brox, "U-Net: Convolutional Networks for Biomedical Image Segmentation," *arXiv:1505.04597 [cs]*, May 2015.
- [13] H. Shan *et al.*, "3-D Convolutional Encoder-Decoder Network for Low-Dose CT via Transfer Learning From a 2-D Trained Network," *IEEE Transactions on Medical Imaging*, vol. 37, no. 6, pp. 1522–1534, Jun. 2018.
- [14] H. Shan *et al.*, "Competitive performance of a modularized deep neural network compared to commercial algorithms for low-dose CT image reconstruction," *Nature Machine Intelligence*, vol. 1, no. 6, p. 269, Jun. 2019.
- [15] H. Chen *et al.*, "Low-Dose CT with a Residual Encoder-Decoder Convolutional Neural Network (RED-CNN)," *IEEE Transactions on Medical Imaging*, vol. 36, no. 12, pp. 2524–2535, Dec. 2017.
- [16] K. H. Jin, M. T. McCann, E. Froustey, and M. Unser, "Deep Convolutional Neural Network for Inverse Problems in Imaging," *IEEE Transactions on Image Processing*, vol. 26, no. 9, pp. 4509–4522, Sep. 2017.
- [17] H. Lee, J. Lee, H. Kim, B. Cho, and S. Cho, "Deep-Neural-Network-Based Sinogram Synthesis for Sparse-View CT Image Reconstruction," *IEEE Transactions on Radiation and Plasma Medical Sciences*, vol. 3, no. 2, pp. 109–119, Mar. 2019.
- [18] T. M. Quan, T. Nguyen-Duc, and W.-K. Jeong, "Compressed Sensing MRI Reconstruction using a Generative Adversarial Network with a Cyclic Loss," *IEEE Transactions on Medical Imaging*, vol. 37, no. 6, pp. 1488–1497, Jun. 2018.
- [19] I. Gulrajani, F. Ahmed, M. Arjovsky, V. Dumoulin, and A. C. Courville, "Improved Training of Wasserstein GANs," in *Advances in Neural Information Processing Systems 30*, I. Guyon, U. V. Luxburg, S. Bengio, H. Wallach, R. Fergus, S. Vishwanathan, and R. Garnett, Eds. Curran Associates, Inc., 2017, pp. 5767–5777.
- [20] H. Chen *et al.*, "Low-dose CT via convolutional neural network," *Biomed Opt Express*, vol. 8, no. 2, pp. 679–694, Jan. 2017.
- [21] J. M. Wolterink, T. Leiner, M. A. Viergever, and I. Išgum, "Generative Adversarial Networks for Noise Reduction in Low-Dose CT," *IEEE Transactions on Medical Imaging*, vol. 36, no. 12, pp. 2536–2545, Dec. 2017.
- [22] "Image quality assessment: from error visibility to structural similarity - IEEE Journals & Magazine." [Online]. Available: <https://ieeexplore.ieee.org/document/1284395/>. [Accessed: 19-Sep-2018].
- [23] C. You *et al.*, "Structurally-Sensitive Multi-Scale Deep Neural Network for Low-Dose CT Denoising," *IEEE Access*, vol. 6, pp. 41839–41855, 2018.
- [24] D. Wu, K. Kim, G. E. Fakhri, and Q. Li, "A Cascaded Convolutional Neural Network for X-ray Low-dose CT Image Denoising," *arXiv:1705.04267 [cs, stat]*, May 2017.
- [25] "Low-Dose CT Image Denoising Using a Generative Adversarial Network With Wasserstein Distance and Perceptual Loss - IEEE Journals & Magazine." [Online]. Available: <https://ieeexplore.ieee.org/abstract/document/8340157>. [Accessed: 12-Apr-2019].
- [26] Z. Wang and A. C. Bovik, "Mean squared error: Love it or leave it? A new look at Signal Fidelity Measures," *IEEE Signal Processing Magazine*, vol. 26, no. 1, pp. 98–117, Jan. 2009.
- [27] "Loss Functions for Image Restoration With Neural Networks - IEEE Journals & Magazine." [Online]. Available: <https://ieeexplore.ieee.org/document/7797130/>. [Accessed: 19-Sep-2018].
- [28] "Low Dose CT Grand Challenge." [Online]. Available: <https://www.aapm.org/grandchallenge/lowdosect/>. [Accessed: 19-Apr-2019].
- [29] M. Abadi *et al.*, "TensorFlow: Large-Scale Machine Learning on Heterogeneous Distributed Systems," p. 19.
- [30] D. P. Kingma and L. J. Ba, "Adam: A Method for Stochastic Optimization," 2015.
- [31] H. Chen *et al.*, "LEARN: Learned Experts' Assessment-Based Reconstruction Network for Sparse-Data CT," *IEEE Transactions on Medical Imaging*, vol. 37, no. 6, pp. 1333–1347, Jun. 2018.
- [32] Q. Yang *et al.*, "Big Data from CT Scanning," 2015.
- [33] C. H. McCollough, M. R. Bruesewitz, and J. M. Kofler, "CT dose reduction and dose management tools: overview of available options," *Radiographics*, vol. 26, no. 2, pp. 503–512, Apr. 2006.
- [34] "Machine learning will transform radiology significantly within the next 5 years - Wang - 2017 - Medical Physics - Wiley Online Library." [Online]. Available: <https://aapm.onlinelibrary.wiley.com/doi/full/10.1002/mp.12204>. [Accessed: 15-May-2019].